Journal of Nuclear Materials 518 (2019) 149–161

Contents lists available at ScienceDirect

Journal of Nuclear Materials

journal homepage: www.elsevier.com/locate/jnucmat

Comparative chemical and structural analyses of two uranium dioxide fuel pellets

Tyler L. Spano [a, c, *], Antonio Simonetti [a], Loretta Corcoran [a], Philip A. Smith [a], Stefanie R. Lewis [a], Peter C. Burns [a, b]

[a] Department of Civil and Environmental Engineering and Earth Sciences, University of Notre Dame, Notre Dame, IN, USA
[b] Department of Chemistry and Biochemistry, University of Notre Dame, Notre Dame, IN, USA
[c] Nuclear Nonproliferation Division, Oak Ridge National Laboratory, Oak Ridge, TN, USA

ARTICLE INFO

Article history:
Received 27 November 2018
Received in revised form
29 January 2019
Accepted 23 February 2019
Available online 28 February 2019

Keywords:
Nuclear forensics
UO_2 fuel
Transition metals
Uranium deposits
Pb isotopes

ABSTRACT

A comparative investigation of the trace element, U and Pb isotopic compositions, and structural attributes of two uranium dioxide fuel pellets was conducted for nuclear forensic applications. One fuel pellet consists of natural UO_2 (0.71% ^{235}U), while the other contains enriched UO_2 (3.98% ^{235}U). Numerous impurities, including transition metals, lanthanides, and main group elements were detected in both fuel pellets with total trace element contents that vary between 9.77 and 11.37 μg/g. The relative abundances of the transition metal impurities in the natural UO_2 fuel pellet are linked to the source U ore and provide important insights into its provenance. X-ray fluorescence spectroscopy was utilized to investigate and compare the macro-(cm)-scale distribution of impurities within each of the fuel pellets. In addition, structural properties of the fuel pellets were examined using powder X-ray diffraction (PXRD) and Raman and infrared spectroscopy. Differences in the intensity of the T_{2g} U-O stretching vibrational mode were observed in the Raman spectra of the fuel pellets. Pb isotope ratios were investigated to potentially differentiate between the natural and enriched UO_2 samples and are linked to the process history of these materials.

1. Introduction

1.1. Uranium, the nuclear fuel cycle, and impurity sources

Nuclear energy currently provides ~20% of the US' electricity demands, and such that 99 nuclear reactors produced 805 billion kWh of electricity in 2016 with fifty-five reactors currently under construction worldwide [1,2]. Illicit interception and malicious use of materials related to the commercial nuclear fuel cycle necessitates the development and implementation of forensic methods [3]. Thus, tracking the provenance of potentially intercepted nuclear material is of the utmost importance. For example, previous studies involving forensic analyses of U-rich materials pertinent to the nuclear fuel cycle, such as uranium ores and ore concentrates (UOC) have relied primarily on trace element and isotopic signatures, which are related to geologic ore formation mechanisms and processing history [4–11]. Trace element impurities in uraninite and UOCs can originate from the numerous steps in fuel fabrication beginning with extraction of U ore from the mine [4,10,12,13]. Similarly, analysis of chemical impurities in uranium dioxide fuel pellets provides insight into the starting composition and chemical and physical fabrication history of these materials [14].

1.2. Uranium ores, extraction methods, enrichment, and deconversion

The sources of U used to fabricate nuclear fuel originate from a wide variety of ore forming mechanisms that give rise to exploitable deposits [15,16]. As a result, U ores commonly display characteristic trace, rare earth element (REE) and isotopic signatures related to the chemical, spatial, and temporal characteristics imparted by the mode of deposition [5,6,17]. The primary ore mineral for U is uraninite, nominally UO_{2+x}. Other ore minerals include coffinite ($U(SiO_4)\cdot nH_2O$), brannerite (UTi_2O_6) and U(VI) minerals resulting from alteration of U(IV) species [18]. Uranium ores are extracted using underground, open pit, or in situ leaching

* Corresponding author.
E-mail address: spanotl@ornl.gov (T.L. Spano).

https://doi.org/10.1016/j.jnucmat.2019.02.038
0022-3115/

techniques [19,20]. Heap leaching may also be used to recover U from low grade ores [21]. Mined U ore subsequently undergoes mechanical and/or chemical extraction to separate U from gangue. Chemical extraction of U from ore generally utilizes acidic or basic leach solutions and may also involve recovery of U as a by-product of phosphate production. U is then precipitated from these chemical systems through neutralization. Heat is applied to obtain the mixed U oxide U_3O_8, yellowcake, or uranium ore concentrate [UOC; 19]. When enriched uranium fuel is necessary, UOC is converted to UF_4 by reactions with H_2 gas and aqueous HF. The resulting UF_4 is then treated with fluorine gas in a fluidized bed reactor to produce gaseous UF_6. Centrifugation or gaseous diffusion techniques enable enrichment in the fissile isotope ^{235}U. An enrichment level of 3–5% ^{235}U is necessary to produce the type of fuel required for commercial nuclear reactors used in the United States. Although numerous distillation procedures are in place for separating impurities from gaseous UF_6, previous works confirm that trace metals and rare earth elements (REEs) may persist during this stage of the nuclear fuel cycle [e.g., 22, 23]. Following enrichment in ^{235}U, UF_6 is converted back to UO_2, typically following one of three processes. Conversion to ammonium diuranate (ADU), and ammonium uranyl carbonate (AUC) are the two most frequently employed processes, followed by the integrated dry route powder process (IDR) [24].

1.3. Fuel fabrication

Increasing burn-up of UO_2 fuel is favorable for reducing nuclear electricity costs and decreasing the volume of used nuclear fuel [25,26]. Burn-up may be improved by decreasing internal pressure in the fuel pellets, which is accomplished by controlling the internal structure with respect to factors of grain size and porosity. In fuels possessing large sized grains (e.g., >20 μm) of UO_2, release of fission gas is decreased and internal pressure increases slowly. Dopants such as TiO_2, Nb_2O_5, CrO_2, CaO and V_2O_5 may be added to increase grain size, porosity, and mean free diffusion path while reducing grain boundary areas [25]. In pellets with controlled porosity, gaseous fission products are better accommodated and the increase of pressure within the fuel is slowed. Composite fuels have also been explored to reduce fission gas release rates [27,28]. Homogenization of UO_2 powder is important for maintaining uniform porosity within fuel pellets and may be accomplished by addition of Zn stearate [29]. Following fabrication, fuel pellets are placed within Zr alloy (Zircaloy) tubes to be inserted in fuel assemblies within nuclear reactors. Fuel assemblies then spend approximately 18 months in a commercial thermal neutron reactor.

1.4. Importance of forensic analysis of nuclear materials

Each of these aforementioned processes has the potential to impart unique forensic signatures in the resulting UO_2 fuel. If similar materials were to fall out of regulatory control, determining the intended use, geologic origin, and anthropogenic provenance of these items is critically important [30]. Early stage fuel cycle materials such as U ores and ore concentrates have been extensively investigated for trace element and isotopic signatures [4,6,17,31,32]. As a result, it is well established that the geochemical origin of U ore imparts unique chemical and isotopic markers. Powder X-ray diffraction (PXRD) and Raman spectroscopy have been utilized to determine structural and morphological attributes of uraninite and uranium oxides [33–36]; more recently these techniques have emerged as nuclear forensic indicators of process history [37–39]. Attributes such as thermal conductivity, oxidation/corrosion susceptibility, dissolution, and thermochemical behavior have been investigated for synthetic UO_2 fuel (SIMFUEL) [26,40–43]. Additionally, there exists a robust body of work regarding the chemical and structural properties of irradiated UO_2 fuel [44–49].

Literature pertaining to the study of fresh (unirradiated) UO_2 fuel intended for use in commercial nuclear reactors is currently limited. As such, the persistence of chemical, structural, and/or isotopic indicators of provenance in late-stage fuel cycle materials remains unclear. To this end, two fuel pellets intended for use in commercial nuclear reactors (Fig. 1) have been comparatively investigated utilizing all analytical techniques available to the authors. The purpose and goals of this work were threefold. First, to differentiate between and examine unique signatures of the natural and enriched fuel pellets. Second, to obtain as much information as possible regarding the geologic origin and process history of the fuel pellets while exploring novel techniques for provenance analysis. Third, report results that can be used for comparative purposes for future forensic investigations of similar materials.

To this end, inductively coupled plasma-mass spectrometry (ICP-MS) was employed to determine and compare trace element signatures within UO_2 fuel pellets. Multicollector (MC)-ICP-MS was used to measure U and Pb isotopic ratios. Powder X-ray diffraction, and Raman and infrared spectroscopic techniques have been

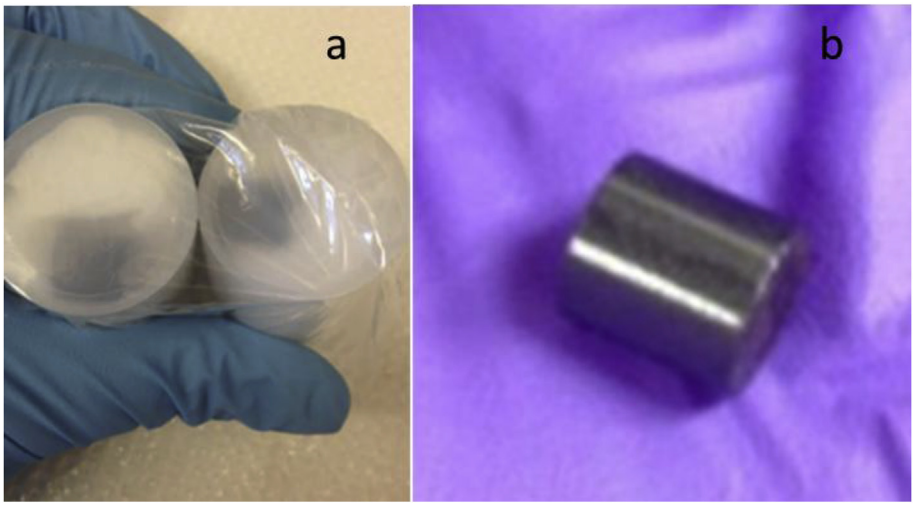

Fig. 1. A. Natural and enriched UO_2 as received. b. Enriched fuel immediately prior to preparation for analyses.

applied to investigate structural properties. In addition, X-ray fluorescence spectroscopy was utilized to obtain information regarding the spatial distribution of impurities.

2. Materials and methods

2.1. Samples

Two UO_2 fuel pellets (Fig. 1) have been examined for their trace element content, U and Pb isotopic compositions, and structural attributes. The first sample consists of U of natural isotopic abundance ($^{235}U = 0.71\%$) and originates from South African mining operations. The locality from which the U for the second fuel pellet, enriched to 3.98% ^{235}U, originates was not provided. Other known properties of the samples investigated in this work are listed in Table 1.

2.2. Structural characterization

2.2.1. Powder X-ray diffraction

Powder X-ray diffraction (PXRD) data were collected using a Bruker D8 Advance Davinci powder diffractometer in Bragg-Brentano configuration. Cu-Kα radiation was produced with an accelerating voltage of 40 kV and 40 mA current. An incident-beam slit of 1.0 mm was reduced by a 0.6 mm slit in combination with 0.02 mm absorber and diffraction (0.6 mm) slits. Data were collected using a step scan with a step velocity of 0.8° min^{-1} in the range of $5–70^\circ$ 2θ using a LynxEye solid-state detector. The reflection positions and intensities of α-Al_2O_3 were used as a calibrant.

2.2.2. Raman spectroscopy

For Raman spectroscopic investigations, UO_2 fuel pellets were affixed on glass slides using carbon tape, and Raman spectra were collected using a Bruker Sentinel linked via fiber optics to a Raman spectrometer. A 785 nm, 100–200 mW laser was focused on the slide-mounted pellets, and data acquisitions were conducted with a high-sensitivity TE-cooled 1024×225 CCD array. Spectra were collected in the range of 80–3200 cm^{-1} over 15 s with 3 signal accumulations. Background measurements were taken at 5 s intervals.

2.2.3. Infrared spectroscopy

Attenuated total reflectance (ATR) infrared spectra of the UO_2 fuel pellets were investigated using a SensIR Technology IllumanatIR-FT-IR microspectrometer. Fragments of fuel pellets were placed on glass slides and the ATR lens was pressed into the samples. Analyses were conducted for 45 s, and data were collected in the range of 650–4000 cm^{-1}.

2.3. Trace element analysis

2.3.1. Trace element concentrations

Inductively coupled plasma mass spectrometry (ICP-MS) was used to determine trace element compositions within UO_2 fuel pellets. For solution mode (SM)-ICP-MS analysis, sample digestion and preparation took place in a class 1000 clean room facility housed within the MITERAC Facility at the University of Notre Dame. Two aliquots of approximately 1.7 g of each of the two UO_2 samples were weighed and placed in pre-cleaned Savillex ® Teflon beakers. For each sample, ~2 mL of double-distilled (DD) concentrated (16 N) HNO_3 was added to the vessel. Samples were then capped and heated at 110 °C for 48 h. Following initial digestion, samples were removed from the hotplate and cooled for 1 h. The beaker was uncapped and any sample residue adhered to the sides of the beakers was rinsed with 18 MΩ cm water. Samples were heated at 150 °C to dryness (~24 h). Approximately 0.5 mL of DD 16 N HNO_3 was added to dried samples. The vessels were recapped and placed on the hotplate for 24 h at 110 °C. The beaker was again uncapped and rinsed with 18 MΩ water. Samples were evaporated to dryness at 150 °C (~24 h). This last step was repeated. Once dry, ~0.5 mL of 16 N HNO_3 was added to each beaker, and samples were immediately heated to dryness at 150 °C. Approximately 2.5 mL of 16 N HNO_3 was added to dry samples and complete dissolution was noted by visual inspection. Dissolved samples were transferred to 125 mL polypropylene bottles and weighed. Ultrapure water was added to bottles until a total weight of approximately 100 g was reached. Samples were then analyzed for trace element concentrations using a spike addition method [50].

For SM-ICP-MS determination of trace element concentrations, samples, standards, and blanks were analyzed in medium mass resolution mode ($M/\Delta M \approx 3000$) using an Attom (Nu Instruments) high resolution (HR)-ICP-MS instrument. At the start of the analytical session, the instrument was tuned and calibrated using a multi-element solution (1 ng/g) in wet plasma mode equipped with a Meinhard concentric nebulizer and cyclonic spray chamber. Additional analytical parameters employed are contained within supporting information.

2.3.2. Trace element distributions

2.3.2.1. X-ray fluorescence spectroscopic mapping. Qualitative chemical analyses and sample maps were acquired to provide an assessment of sample homogeneity using an EDAX Orbis PC micro-XRF system equipped with a 50 kV, 50 W Rh tube, a 30 μm ultra-high intensity poly-capillary optic, and a 30 mm^2 silicon drift detector (Apollo XRF ML-30). The position of the Cu-Kα line from a standard wafer was used as a calibrant. Each UO_2 fuel pellet was brought into focus and photographed using a CCD camera. X-rays were generated using a 30 kV voltage and 0.3 mA current.

2.4. U and Pb isotope measurements

2.4.1. U separations

Sample preparation for isotopic investigations also took place in a class 1000 clean room facility and involved transferring dissolved aliquots of the UO_2 to pre-cleaned Savillex ® Teflon beakers, which were subsequently placed on a hot plate at 110 °C and evaporated to dryness. Prior to U ion exchange chemistry, samples were re-dissolved into 0.5 mL DD 4 M HNO_3. BioRad 5" columns were rinsed with several aliquots of 18 MΩ cm water and loaded with 1 mL UTEVA (100–150 μm) resin. Columns were then primed with 2 mL of 18 MΩ water and 4 mL 4 M HNO_3. Redissolved samples were loaded onto resin beds and then rinsed with 4.5 mL of 4 M HNO_3. Columns loaded with sample aliquots were then rinsed with 1.5 mL of 9 M HCl, followed by 5 mL of 5 M HCl. U was eluted to pre-cleaned Savillex ® Teflon beakers upon addition of 6.5 mL 0.1 M HCl. U samples were then evaporated to dryness at 110 °C and subsequently re-dissolved into 1 mL double-distilled concentrated (16 N) HNO_3 at 110 °C [51]. Lastly, samples were diluted in 2% HNO_3 to ~50 ng/g solutions for MC-ICP-MS analysis.

Table 1
Samples investigated in this work.

	Natural	Enriched
Weight (g)	6.0149	6.0581
Average Enrichment (%^{235}U)	0.71	3.95
Mass^{235}U (g)	0.038	0.212
Country of Origin	South Africa	Unknown

2.4.2. Pb separations

Pb isotope investigations were initially preceded by a two-step anion exchange method [52] in which aliquots of previously dissolved UO_2 were transferred to pre-cleaned Savillex® Teflon beakers and evaporated to dryness. Due to the high U content (~88 wt% in solid samples) and low Pb concentrations (~25 ng/g), evaporating samples proved problematic. The method developed by Manhes, Minster et al. [52] requires evaporated samples to be redissolved in ~0.5 mL of 0.8 N HBr prior to loading aliquots on the column, however, precipitation of large quantities of uranyl nitrate precluded dissolution of samples in the HBr matrix. To this end, the method for U separations described in Section 2.4.1 was modified and applied to extract excess U from solutions prior to Pb separations. For the natural and enriched samples, aliquots of approximately 2.5 mL were evaporated to dryness and redissolved in 0.5 mL 4 M HNO_3. As described above, BioRad columns were prepared and loaded with sample aliquots. The addition of six 1 mL rinses with 9 M HCl following the initial 9 M washes described by Pollington, Kinman et al. [51] proved to be sufficient for Pb removal. All eluents prior to elution of U via addition of 0.1 M HCl were collected and evaporated to dryness. Samples were once again dissolved in ~0.5 mL of 0.8 N HBr and loaded into pre-cleaned and conditioned columns. The columns were then repeatedly rinsed with 0.8 N HBr followed by elution and collection of Pb via addition of 0.7 mL of 6 N HCl. Subsequent to ion exchange separations, samples were evaporated to dryness and redissolved in a 2% (v/v) HNO_3 solution spiked with ~5 ppb Tl immediately prior to MC-ICP-MS analysis.

2.5. U and Pb isotope analysis

Uranium and lead isotope measurements were conducted using a NuPlasma II MC-ICP-MS instrument. Sample and standard solutions were self-aspirated into the plasma using a desolvating nebulizing system (DSN-100 from Nu Instruments). U isotope data were acquired in static, multi-collection mode using 2 F collectors for measurement of ^{238}U and ^{235}U ion signals, and two discrete dynode secondary electron multiplier (SEM) for acquisition of ^{234}U and ^{236}U following protocols outlined by Brennecka et al. [31] and Bopp et al. [53]. The SEM is equipped with a retardation/deceleration lens filter that limits the abundance sensitivity to ~500 ppb, whereas the latter value is < 5 ppm for all Faraday collectors as the recorded baseline measurement at mass 237 with a large ^{238}U ion signal. Analyses of CRM 112 A (New Brunswick Laboratory) U isotope standard bracketed each sample so as to monitor for instrumental mass bias and drift. For standards and samples, U isotope data were collected for a total of 400 s, consisting of 40 scans of 10 s integrations each. Mass bias corrections using the exponential law were applied to samples based on the known isotopic ratios of $^{238}U/^{235}U$, $^{238}U/^{234}U$, and $^{235}U/^{234}U$ in CRM 112 A. Internal in-run precision (2σ level) associated with individual U isotope measurements are typically several orders of magnitude better than the external reproducibility. The relative standard deviation reported for U isotope measurements are based on repeated analysis of CRM 112 A during data acquisition for the fuel pellet samples. Moreover, U isotope standards IRMM-184 and IRMM-185 were also analyzed during the period of study using the same standard sample bracketing technique as was utilized for the fuel pellet samples. The results are provided in the supporting information and include the calculated, average values for the U isotope ratios and their associated standard deviations (2σ level), and these are consistent with recommended/accepted values for both standards from the literature [54–56].

Pb isotope data were also collected in static multi-collection mode, with masses of 202 (Hg), 203 (Tl), 204 (Pb and Hg), 205 (Tl), 206 (Pb), 207 (Pb), and 208 (Pb) monitored simultaneously on Faraday cups following a procedure outlined by Simonetti et al. [57]. Each analysis involved acquisition of one block of data consisting of 25 10 s scans, preceded by a 30 s baseline measurement. Total Pb beams which correspond to the sum of all Pb isotope signals under investigation were 5.4 V, and 4.58 V for the natural and enriched UO_2 fuel pellet samples, respectively. On-line corrections for the ^{204}Hg interference on ^{204}Pb were conducted during analyses and mass bias corrections were applied to samples using the exponential law based upon the accepted isotopic ratios of NIST SRM 997 thallium isotopic standard. Offline blank subtractions were also conducted to correct for Pb contamination that may have taken place during removal of the U matrix.

3. Results

3.1. Structural analysis

3.1.1. Powder X-ray diffraction

Powder X-ray diffractograms for UO_2 fuel pellets obtained in this study are shown in Fig. 2 and are nearly identical to the mineral uraninite [58]. Five diffraction peaks are observed for both fuel pellets at ~28, 32, 46, 55, and 58° 2θ which correspond to the 111, 200, 220, 311, and 222 reflections respectively [59]. Diffraction data for the fuel pellets show evidence of peak splitting, particularly in the 220 and 200 reflections (Fig. 3).

3.1.2. Raman and infrared spectroscopy

The Raman spectra for the fuel pellets are shown in Fig. 4. Both spectra display the T_{2g} U-O stretching vibrational mode at approximately 445 cm^{-1} which is characteristic of fluorite structured UO_2 and is caused by the triply degenerate T_{2g} Raman active vibration [60]. Although visible in both spectra, the response of Raman intensity of this vibrational mode as a function of laser power differs for the two samples (Fig. 5a and b). As shown in Fig. 5c, although linearity of signal intensity is maintained for both samples while laser power is increased, regression of these two trends indicates that the intensity of the T_{2g} peak in a sample of enriched U is less responsive to an increase in laser power than a sample of natural isotopic abundance.

Low intensity vibrational modes are present at ~640 cm^{-1} and

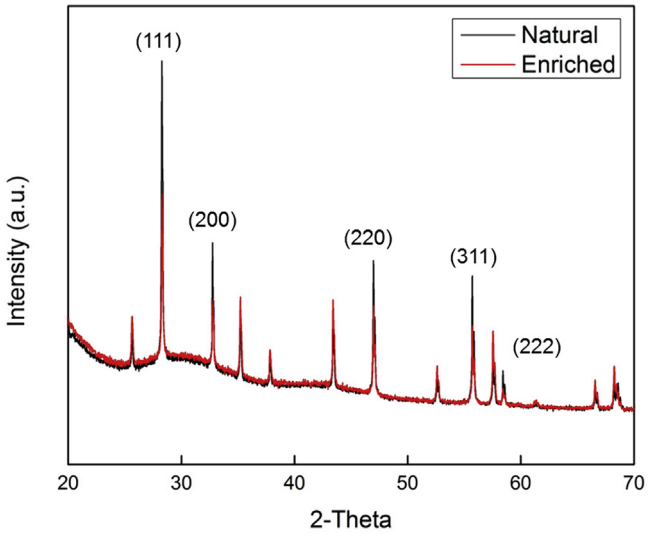

Fig. 2. Powder X-ray diffractograms for natural and enriched UO_2 fuel pellets. Labeled reflections are those from UO_2, all others originate from the α-Al_2O_3 internal standard.

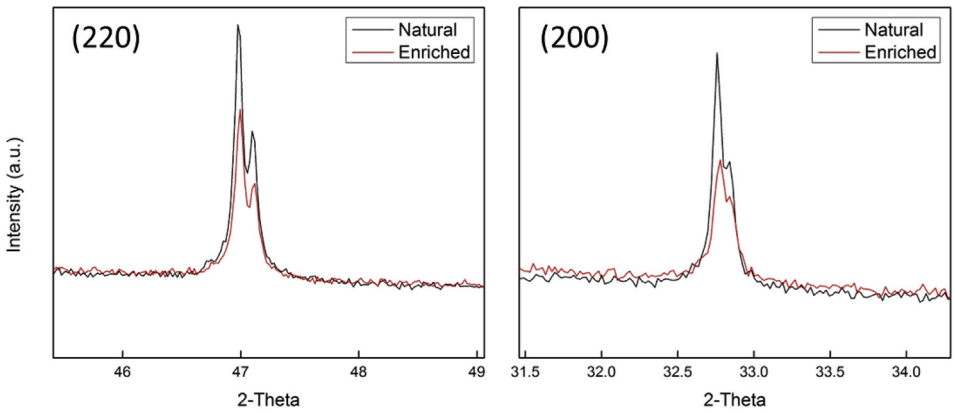

Fig. 3. Peak splitting observed in powder X-ray diffractograms of UO_2 fuel pellets.

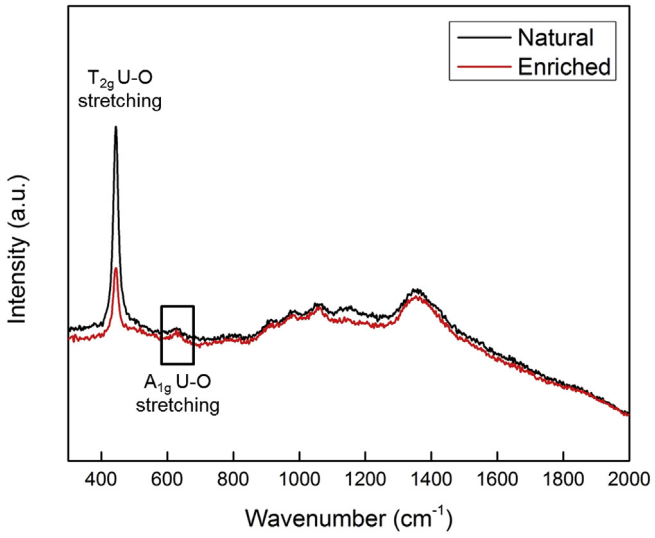

Fig. 4. Raman spectra for samples investigated in this study.

are likely attributed the A_{1g} U-O stretching modes resulting from structural accommodation of excess oxygen and subsequent relaxation of selection rules [36,61]. While it is possible that contributions to this signal arise from surface oxidation to U_3O_8 [61], this assignment is unlikely as Raman spectra collected for both exterior and interior (freshly broken prior to analysis) of fragments of UO_2 samples yielded identical vibrational spectra.

In stoichiometric to slightly hyperstoichiometric UO_2, an additional vibrational mode, located at approximately 1150 cm^{-1} (Figs. 4–5) has been reported. This is considered a fingerprint of the quasi-perfect fluorite structure [61]. Attributed to $\Gamma_5 \rightarrow \Gamma_3$ crystalline-electric-field (CEF) transitions, this vibrational mode was not observed in the fuel pellets investigated here.

Infrared spectroscopic investigations of the two fuel pellets yielded nearly identical results. Weak vibrational modes were observed at 667 and 668.9 cm^{-1} for the natural and enriched fuel pellets respectively (Supplemental Information, Figure S1). Also present for the natural and enriched fuel pellets are vibrational modes at 758.2 and 760.1 cm^{-1}.

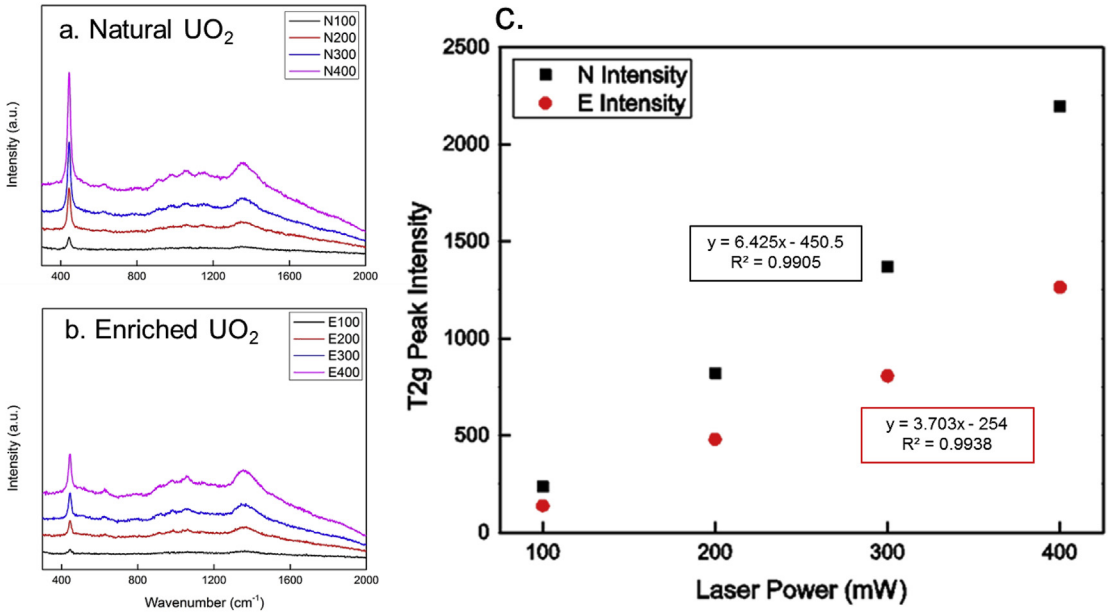

Fig. 5. A, b. Raman spectra collected with various laser powers for natural (top left) and enriched (bottom left) samples. c. Observed intensity of the T_{2g} vibrational mode as a function of increasing laser power.

3.2. Trace element content and distribution

3.2.1. Impurities in UO_2 fuel

The fuel pellets examined in this study contain numerous trace element impurities as summarized in Table 2 and Fig. 6. Very low quantities of Sc, Ga, Ho, Lu, and Hf were observed in the fuel pellet of natural U isotopic abundance and are below detection limits for the enriched fuel pellet. Conversely, Tb, Dy, Er, Tm, and Ta were detected only in the enriched fuel pellet. SM-ICP-MS analyses reveal that Ca, V, Fe, Cr, Co, Ni, Cu, Sr, Zr, Nb, Mo, Sn, Sb, Ba, La, Ce, Pr, Nd, Sm, Eu, Gd, Yb, W, Pb, Bi and Th are present in variable concentrations (0.03–3.4 μg/g) within both samples. All observed impurities fall below the accepted impurity values for UF_6 prepared for enrichment with the exception of W in the enriched fuel pellet [62].

3.2.2. Trace element distributions: X-ray fluorescence spectroscopic mapping

X-ray fluorescence spectroscopic mapping was utilized to examine the macro-(cm)- scale distribution of selected trace elements in fuel pellet samples. Montage images of the fragments of the fuel pellets investigated using XRF mapping are shown in Fig. 7a. High resolution elemental maps were generated for Cr, Mo, W, and Zr for exterior and interior areas of the natural and enriched fuel pellets (Fig. 7b–e). Areas of elevated Cr content were homogeneously distributed throughout the exterior of both natural and enriched fuel pellets. The interior of the enriched fuel pellet shows similar Cr distribution to the exterior of both samples, whereas the interior of the natural fuel pellet exhibits a relative enrichment in Cr (Fig. 7b). Distribution of Mo is variable when comparing exterior maps to those generated from the interior of fuel pellet samples. The interior of the enriched fuel pellet shows lower concentrations of Mo when compared to the exterior of the same sample, and to the external and internal maps of the natural sample (Fig. 7c). Conversely, W appears to be homogeneously distributed throughout the interior and exterior areas of the natural and enriched fuel pellets (Fig. 7d). Zr is highest in the interior of the enriched fuel pellet compared with the other sampling areas (Fig. 7e).

Table 2
Trace element contents of UO_2 fuel pellets investigated in this study.

Element	Enriched (ng/g)	Natural (ng/g)
Li	bdl	bdl
Be	bdl	bdl
Ca	5.89	8.45
Sc	bdl	1.14
V	49.64	313.76
Cr	2715.80	3468.84
Fe	70.40	77.43
Co	40.97	72.41
Ni	1057.76	1412.16
Cu	211.28	415.52
Zn	bdl	bdl
Ga	bdl	0.11
Rb	bdl	bdl
Sr	2.53	7.72
Y	bdl	bdl
Zr	8.26	2437.27
Nb	2.68	3.15
Mo	1453.41	788.26
Sn	553.53	1536.38
Sb	5.54	7.26
Cs	bdl	bdl
Ba	20.35	28.15
La	38.56	46.02
Ce	3.45	4.71
Pr	0.46	0.90
Nd	0.91	2.53
Sm	1.54	1.42
Eu	0.68	0.62
Gd	4.08	2.86
Tb	0.07	bdl
Dy	0.82	bdl
Ho	bdl	0.09
Er	0.90	bdl
Tm	0.03	bdl
Yb	2.14	1.18
Lu	bdl	0.13
Hf	bdl	4.60
Ta	9.15	bdl
W	3171.06	507.93
Pb	11.10	25.24
Bi	2.03	2.13
Th	384.63	248.11

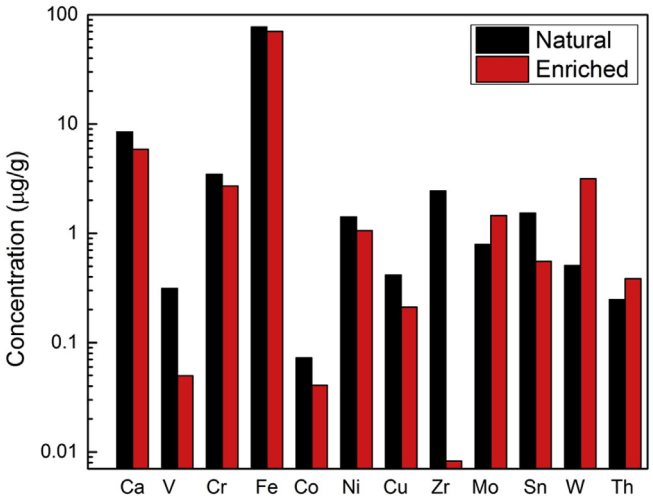

Fig. 6. Selected trace element concentrations (log scale) observed in fuel pellets.

3.3. Isotopic analyses

3.3.1. Lead isotope analysis

Results of lead isotope analyses and their corresponding analytical uncertainties are contained within Table 3. Measured $^{208}Pb/^{204}Pb$, $^{207}Pb/^{204}Pb$, $^{206}Pb/^{204}Pb$, $^{206}Pb/^{207}Pb$, $^{208}Pb/^{206}Pb$, and $^{208}Pb/^{207}Pb$ values coincide with the isotopic composition of Pb ores originating from North American Mississippi Valley type Pb deposits [Fig. 8, modified from 63].

3.3.2. Uranium isotope analysis

Uranium isotope measurements and associated analytical uncertainties (2σ level) for the natural and enriched fuel pellets yielded $^{238}U/^{235}U$ values of 137.75 ± 0.08 and 24.18 ± 0.08, respectively. These results equate to ^{235}U enrichments of 0.721% in the natural sample, and 3.970% for the enriched sample. The natural and enriched fuel pellets have $^{238}U/^{234}U$ values of 18746.1 ± 1.2 and 2822.0 ± 1.2, respectively. $^{235}U/^{234}U$ values and associated analytical uncertainties are 136.05 ± 1.18, and 116.69 ± 1.18 for the natural and enriched fuel pellets, respectively. These results are summarized in Table 4.

4. Discussion

4.1. Structural distortions in UO_2 fuel

Splitting of reflections in the diffraction pattern of both the

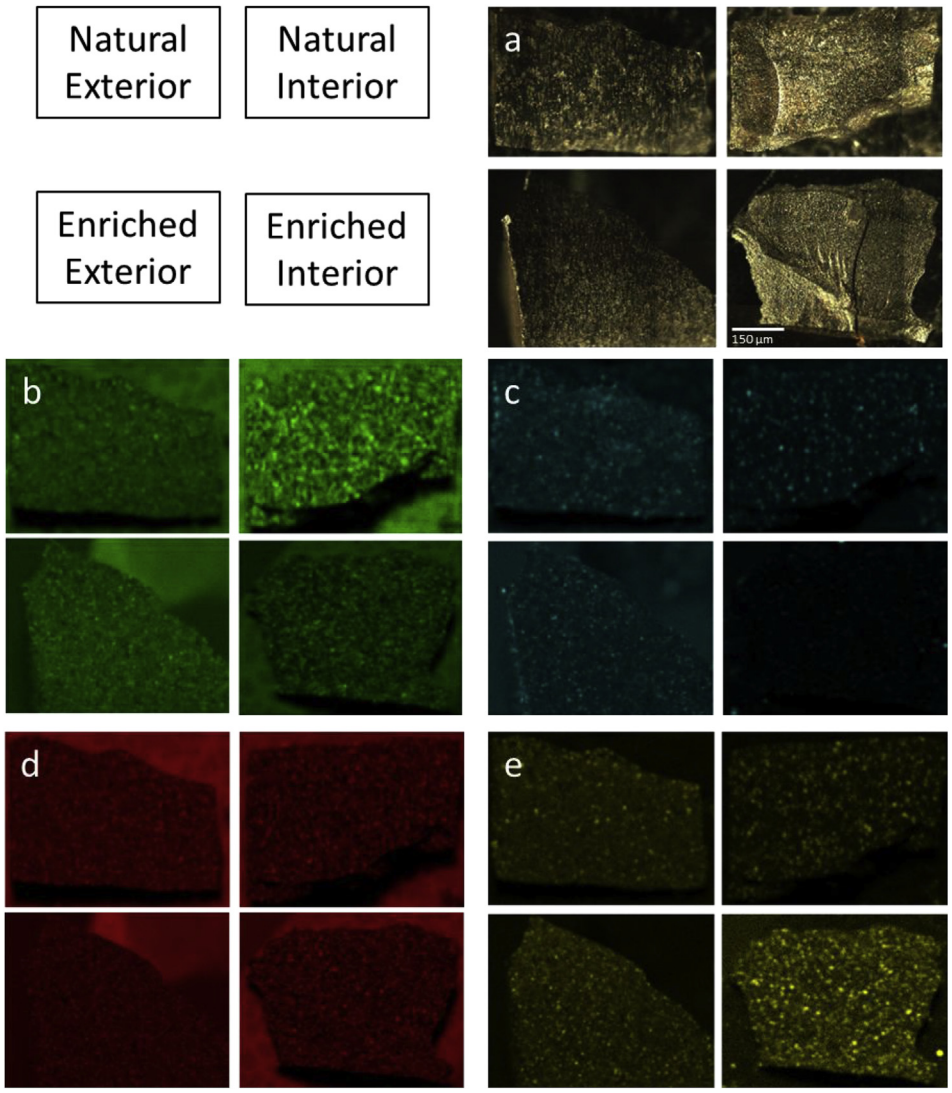

Fig. 7. A. Montage images and X-ray fluorescence spectroscopic maps of b. Cr (green), c. Mo (cyan), d. W (red), and e. Zr (yellow) as observed on the exterior and interior (freshly broken fragments) of natural and enriched fuel pellets. (For interpretation of the references to colour in this figure legend, the reader is referred to the Web version of this article.)

isotopically natural and enriched fuel pellets likely indicates a phase transition to tetragonal from cubic symmetry, or potentially a mixture of two isometric UO_2 phases with differing unit cell parameters [Fig. 3 [64,65]]. Further confirming this assessment is the intact 111 reflection, which, upon transformation from a cubic to tetragonal phase, will not split. Whether originating from cubic to tetragonal transitions or from the presence of multiple isometric UO_2 phases, this observation indicates that structural transformations and defects are present/occurring in both fuel pellets examined here.

In addition to peak splitting observed using PXRD, evidence of phase transformations and deviation from stoichiometric, ideally fluorite-structured UO_2 is indicated by Raman spectroscopy. Reduced intensity of the T_{2g} mode has been found to correlate with increasing incorporation of oxygen, and subsequent progression towards hyperstoichiometry [36,48]. The differences in the Raman spectra indicate that the enriched fuel pellet is more susceptible to structural distortion than the natural sample. As a result, the slope of the intensity of the T_{2g} vibrational mode of a potentially seized uranium oxide sample when examined as a function of increasing laser power may be compared with the linear regressions presented in this work as means to rapidly identify the intended use (enrichment level) of fuel pellets that have fallen out of regulatory control. Despite unique Raman signal responses observed for the fuel pellets investigated here, the cause of these signal variations requires further investigation beyond the scope of this work.

Table 3
Pb isotope compositions of UO_2 fuel pellets.

Sample	$^{208}Pb/^{204}Pb$	$^{207}Pb/^{204}Pb$	$^{206}Pb/^{204}Pb$	$^{206}Pb/^{207}Pb$	$^{208}Pb/^{206}Pb$	$^{208}Pb/^{207}Pb$
Natural	37.734	15.713	20.089	1.278	1.878	2.401
Enriched	37.929	15.693	19.582	1.248	1.937	2.417
Standard Error	5.34E-04	2.35E-04	2.65E-04	8.61E-06	1.77E-05	5.49E-04

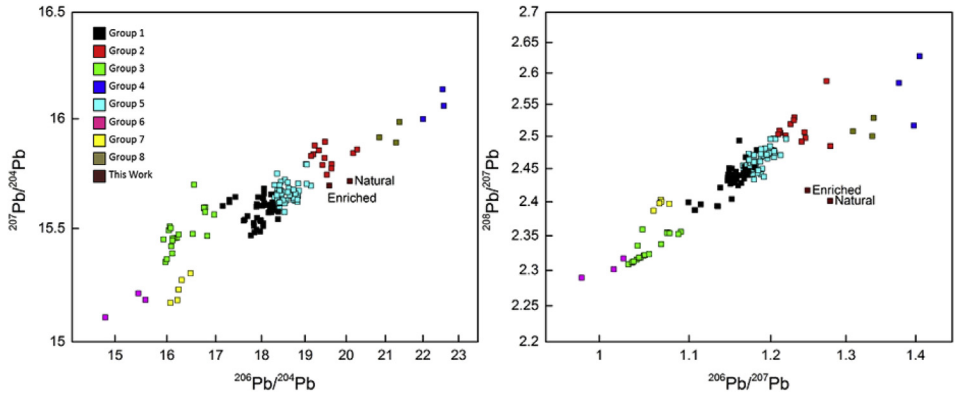

Fig. 8. Pb isotopic compositions and associated analytical uncertainties of UO_2 fuel pellets. Groups correspond to statistical clusters among global lead deposits based upon principal components analysis. The Pb isotopic composition of both fuel pellets coincide with the expected values for Pb ores originating from North American Mississippi Valley type deposits (red and cyan). Modified from Sangster et al., 2000. (For interpretation of the references to colour in this figure legend, the reader is referred to the Web version of this article.)

The absence of the ~1150 cm^{-1} vibrational mode may indicate that despite a greater degree of hyperstoichiometry in the enriched sample as observed via an examination of the T_{2g} peak, defects in the fluorite structure are present in both fuel pellets. Similar to the absence of the $\Gamma_5 \rightarrow \Gamma_3$ CEF transition in the Raman spectra, increased ordering of lattice oxygen and deviation from the ideal fluorite structure is evidenced by results from IR spectroscopy. The absorption bands at ~668 cm^{-1} likely result from local β-U_3O_7 or β-U_4O_9/[$U_4O_{(8/3)}O_4$] ordering in the normally fluorite-structured UO_2 [66–69].

4.2. Trace element contents of UO_2 fuel

4.2.1. Forensic implications

Separation and detection of impurities in fuel cycle materials (e.g., UF_6, UO_3, U_3O_8) has been the focus of numerous investigations [14,26,70,71]. Despite well-defined analytical methods for determining trace element contents in U-materials from early stages in the nuclear fuel cycle (e.g.; uranium ores and ore concentrates), the residual geologic and process-related anthropogenic sources of these impurities and thus, forensic implications for their presence are not addressed in detail [8,10]. While it is probable that many of the trace elements observed in the samples examined in this study relate to the geologic origin of the U used in fuel fabrication, the current lack of knowledge regarding potential process-related impurity sources of trace element contents within UO_2 fuel warrants discussion here.

To determine the trace element contents that are unique to each UO_2 fuel pellet, impurities detected in both samples are shown in Fig. 9. Trace element constituents that were below detection limits for either sample are not included. Each point in Fig. 9 represents the concentration (μg/g) of a given element in the enriched sample plotted as a function of its corresponding content in the natural UO_2 fuel. A prominent 1:1 linear trend with few deviations is observed for most elements. For elements that exhibit deviation from unity, the orthogonal distance between each pair of trace element concentrations and the line representing constant abundances were calculated and are summarized in Table S3 (Supporting Information). These calculations indicate that Ca, Fe, W, Zr, Sn, Cr, Mo, Ni, V, and Cu contents are important indicators that enable distinguishing between the natural and enriched fuel studied in this work.

4.2.1.1. Transition metals in UO_2 fuel. Given the depletion in rare earth elements (REEs) reported here and in previous studies of a similar nature, this then necessitates examination of other possible trace element signatures for provenance identification (e.g., U deposit type, locality) of the U used in UO_2 fuel. To explore the possibility that trace element impurities observed in fuel are indeed artifacts (and forensic indicators) arising from the source U ore, binary plots were generated for each combination of W, Cr, Mo, Ni and V. In addition to trace element contents observed for fuel pellets in this work, uraninite samples from granite-related, sandstone, tabular sandstone, unconformity, metamorphite, and intrusive U deposit types are also reported in Fig. 10 [7,17]. Overlap between fuel pellets and intrusive deposits is observed (Fig. 10). This is of particular interest as the source U ore for the natural fuel pellet is South African, and deposits in this province are classified as intrusive [5,16]. The lack of coincidence observed in binary plots containing Cr may result from addition of or contamination by this element during fuel fabrication.

To further explore the possibility that transition metal signatures may be applied to determine the origin of the U contained within the fuel pellets, transition metal ratios for several South African U deposits are compared with those of the UO_2 fuel. Transition metal contents reported for uraninites from Vall Reefs, Stilfontein, West Driefontein, Saaiplass, and President Steyn Mines are compared with UO_2 fuel [72]. For each possible combination of transition metal ratios (e.g. V/Cr, V/Fe, etc.) the average value for each locality was determined (Table S4, Supporting Information). Binary plots were then employed to compare the ratio signatures in the UO_2 fuel pellets with the averages of the South African U mines

Table 4
U isotope composition of UO_2 fuel pellets.

Information Provided with Pellets				Measured			
Sample	$^{235}U/^{238}U$ Average Enrichment	$^{235}U/^{238}U$ Maximum Enrichment	Standard Deviation Enrichment	$^{235}U/^{238}U$	$^{234}U/^{238}U$	$^{234}U/^{235}U$	^{235}U wt%
Natural	0.00710	0.00713	±0.00002	7.26E-03	5.33E-05	7.35E-03	0.72070
Enriched	0.00395	0.03978	±.00011	4.14E-02	3.54E-04	8.57E-03	3.97000

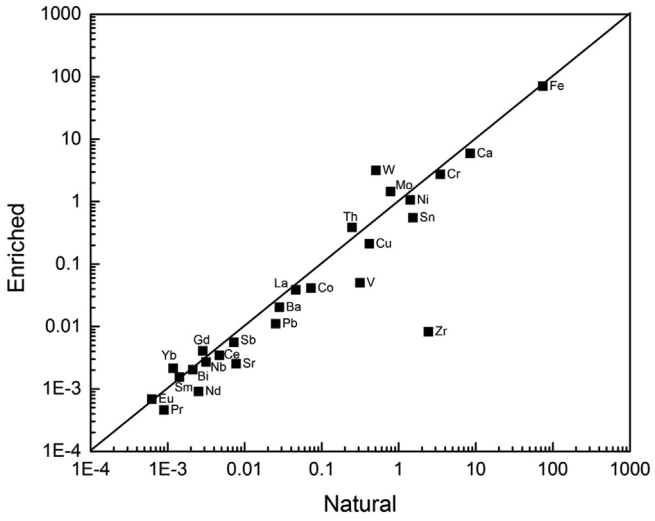

Fig. 9. Trace element concentrations in natural and enriched UO_2 fuel pellets. Deviations from the diagonal line represent unique signatures in natural (below line) and enriched (above line) fuel pellets.

listed above (Fig. 11). For both the natural and enriched fuel pellets, transition metal ratio values appear to correlate with those of uraninites from Saaiplass and West Driefontein mines. Although the linear regression for each of the binary plots for transition metal ratios of South African U mines and UO_2 fuel results in the highest correlation coefficient and slope closest to unity for West Driefontein Mine, depletion in several transition metals (and resulting lack of available ratios for comparison) leads to the conclusion that both fuel pellets originate from the Saaiplass Mine, or from U deposits in close proximity thereof.

4.2.1.2. Possible anthropogenic impurity sources. Although addition of W to UO_2 has been shown to extend fuel burn-up and lead to more economically favorable fuel materials in experimental materials [28] a likely source of W may arise from the use of sintering vessels and related materials composed of W-based alloys [73]. Another, less-likely scenario is the fabrication of structural components that contain trace amounts of W in the same facility where fuel production is occurring [74].

Zr is an important constituent of nuclear reactors and is a primary component of the cladding that contains the fuel pellets during burn-up within a reactor. Zircaloys are resistant to corrosion at high temperatures and serve as a protective barrier between fuel pellets and water/steam during reactor operations. Furthermore, the low neutron absorption cross section of Zr results in this element being used in structural components of reactor cores [74]. Similar to Zr and W, Sn is utilized in fabrication of reactor materials, including Zircaloy cladding. This is due to the ability of Sn to improve corrosion resistance of cladding components [75].

The presence of Cr was detected in both fuel pellets, with a greater concentration in the fuel pellet of natural isotopic U abundance (3.47 μg/g). Based upon results shown in Fig. 10, the Cr content of the fuel pellets does not appear to be related to residual impurities from the geologic origin of U ores used to produce the pellets. Cr addition to UO_2 fuel is well documented in experimental literature as an additive capable of modifying the initial pellet microstructure and altering diffusion behavior of both gaseous and solid fission products during fuel burn-up [27,76,77]. Additionally, Cr is used in fabrication of brick refractory, which is employed to line furnaces and kilns. Thus, it is possible that Cr contamination of UO_2 fuel occurs during sintering [78].

The addition of Mo to U oxide promotes corrosion resistance, particularly from high temperature waters during reactor operations. Addition of Mo also enables retention of the body-centered-cubic γ phase during irradiation which improves in-reactor stability of fuel, thereby increasing irradiation performance parameters [25]. Similar to tungsten, molybdenum is another primary material contained within furnace boats for pellet sintering. In addition to contributions from the trace element content of U ores used to fabricate fuel, Mo may also exist in fuel pellets as an artifact of this process. Similarly, Ni and Cu impurities may arise from the use of Monel cylinders that are employed to filter UO_2 powder generated during IDR deconversion processes [79]. Ni-based alloys are characterized by high thermal stability and may also be used in nuclear reactor structure materials [74].

The vanadium content (0.31 μg/g) for the fuel pellet of natural U isotopic abundance is approximately six times higher than that contained within the enriched sample (0.05 μg/g). Given that uranyl vanadate minerals are ubiquitous within the alteration zones of numerous U deposits and are mined as sources for U ore [80–83], it is likely that this higher V abundance in the natural U pellet is the result of incomplete separation of V during early ore processing.

4.3. Pb isotopes

Examination of the Pb isotopic compositions of the natural and enriched UO_2 fuel indicate that regardless of where mining and enrichment took place, fuel fabrication was either conducted in the United States, or fabricated using materials produced therein. This is evidenced by overlap/close proximity the measured Pb isotopic ratios for the fuel pellets with the expected isotopic composition of anthropogenic sources of Pb ores within the United States; this despite being composed of South African U ores [63]. Although Pb isotope overprinting during fuel fabrication inhibits determining the geologic provenance of fuel pellet constituent materials, identification of the location at which manufacturing/fabrication of manufacture components took place is possible. In addition to obtaining forensic information regarding the provenance of fuel fabrication, the effective chromatographic separation of Pb from U-rich matrices has been demonstrated.

4.4. U isotopes

Results of U isotope analyses coincide with expected enrichment values that were provided upon receipt of the fuel pellets. The sample enriched to 3.97 wt% ^{235}U was likely intended for use in either a boiling or pressurized water type commercial nuclear reactor as are utilized in the United States. Conversely, the 0.71 wt% ^{235}U enrichment level observed in the other sample would likely be used in a pressurized heavy-water reactor (e.g. CANDU (Canada Deuterium Uranium)).

5. Summary and conclusions

In this work, structural attributes, trace element contents and distributions, and the U and Pb isotopic compositions of two UO_2 fuel pellets have been explored for nuclear forensic applications. Powder X-ray diffraction and Raman spectroscopic investigations have illuminated differences between short-range ordering in the crystalline structure of samples examined in this study. Evidence of peak splitting, which corresponds to reduced symmetry in the structure of UO_2 has been observed in both samples. Additionally, differences in Raman signal response to increasing laser power have been detected when comparing natural and enriched fuel pellets.

Trace element abundances indicate that although numerous

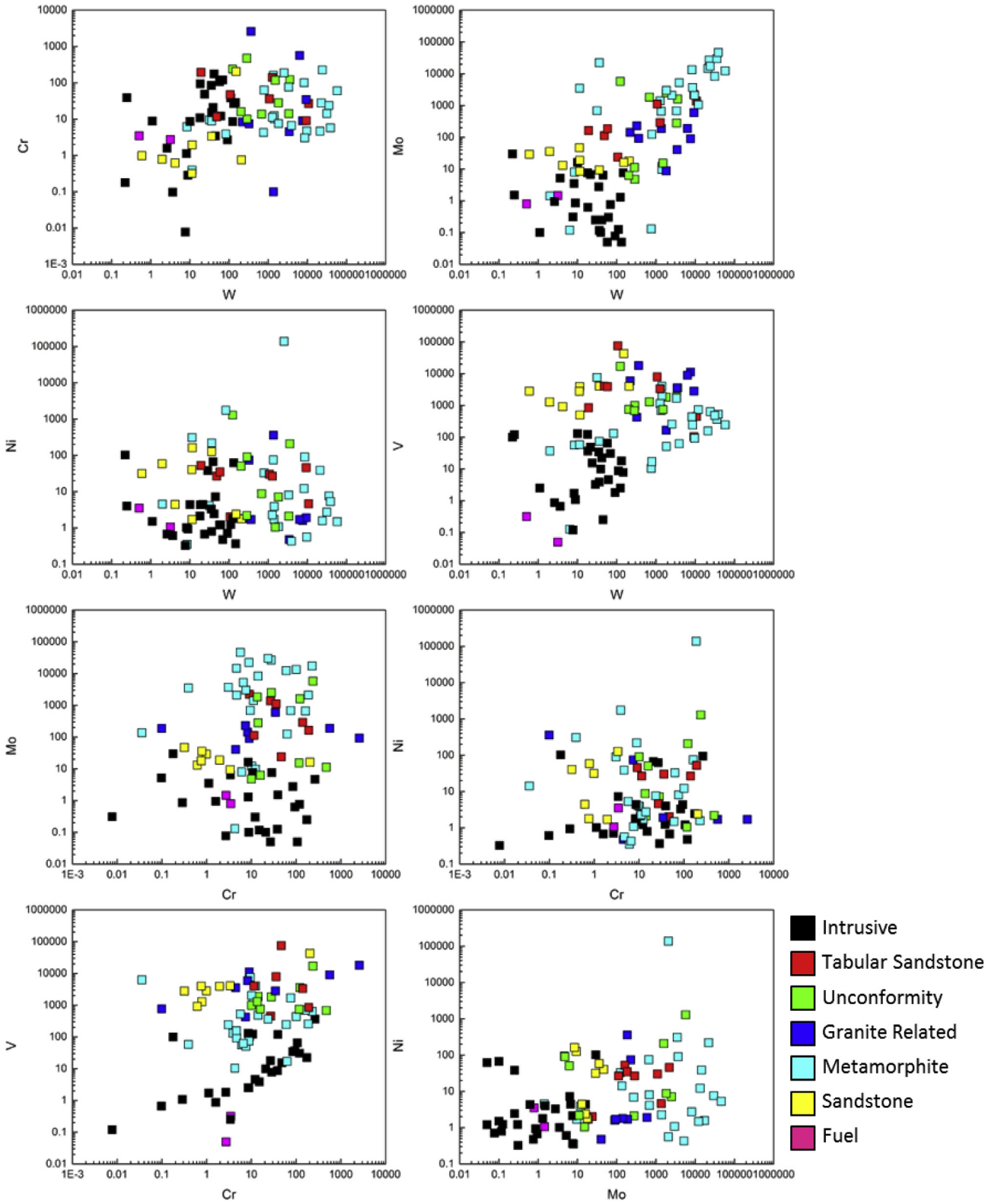

Fig. 10. Selected transition metal binary plots for uraninite and UO_2 fuel. Colors indicate U deposit types. (For interpretation of the references to colour in this figure legend, the reader is referred to the Web version of this article.)

impurities are present in both UO_2 fuel pellets, each sample possesses a distinct chemical signature (e.g., Sc, Ga, Ho, Lu, and Hf in the natural sample, Tb, Dy, Er, Tm, and Ta in the enriched fuel). Transition metal contents and ratios have been examined and applied to determine that the U used for fuel fabrication originates from an intrusive ore source; likely Saaiplass mine in South Africa. Although the sample size is limited, these elemental compositions appear to be unique signatures for each fuel pellet. Furthermore,

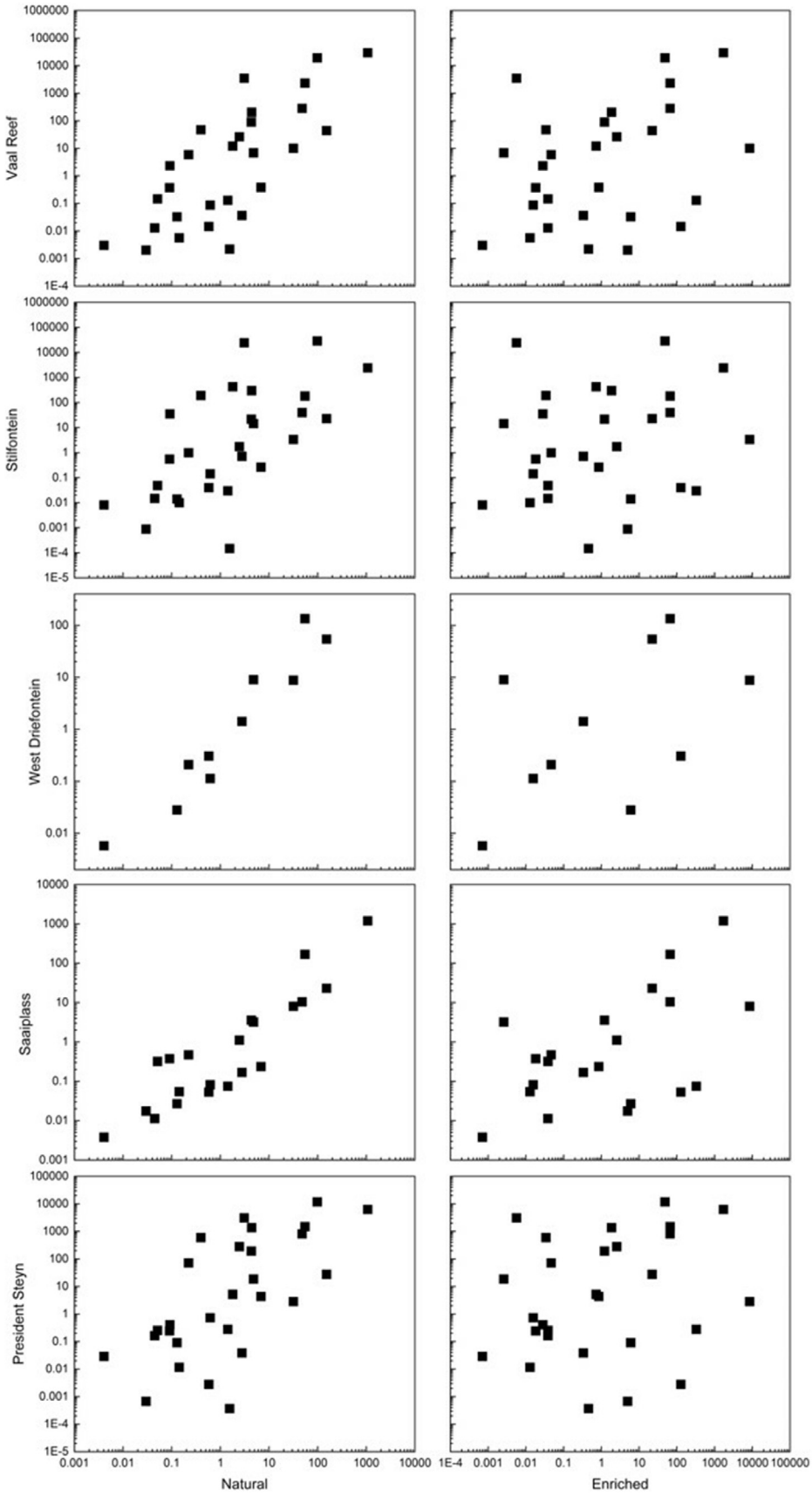

Fig. 11. Transition metal ratio binary plots for natural and enriched fuel pellets and South African U localities.

the W concentrations in the enriched sample investigated in this work are higher than standard limits (ASTM), indicating that contamination may have occurred after deconversion from UF_6. Variations in the spatial distribution of trace elements was observed via X-ray fluorescence spectroscopic mapping, and unique Pb isotopic signatures can assist in determining the process history of nuclear material that has fallen out of regulatory control. Lastly, U isotope signatures were found to be consistent with enrichment levels provided for the fuel pellets examined in this work.

Acknowledgements

We thank Dr. Ginger E. Sigmon for making this work possible, and two anonymous reviewers for their helpful comments. This research was supported by the U.S. Department of Homeland Security grant DHS-14-DN-077-ARI, and the ND Energy Postdoctoral Fellowship Program. Analyses were conducted at the Midwest Isotopic and Trace Element Research Center (MITERAC), the Center for Environmental Science and Technology (CEST), the Actinide Center of Excellence (ACE), and the ND Energy Materials Characterization Facility (MCF) at the University of Notre Dame.

Appendix A. Supplementary data

Supplementary data to this article can be found online at https://doi.org/10.1016/j.jnucmat.2019.02.038.

References

[1] W.N. Association, Nuclear Power in the USA, 2018. Available from: http://www.world-nuclear.org/info/Country-Profiles/Countries-T-Z/USA-Nuclear-Power/.
[2] P. Database, Reactor Status Reports, International Atomic Energy Agency, 2019.
[3] Mayer, K., Wallenius M., and Ray I.. Tracing the origin of diverted or stolen nuclear material through nuclear forensic investigations. in Verifying Treaty Compliance. 2006. Berlin, Heidelberg: Springer Berlin Heidelberg.
[4] T.L. Spano, et al., Trace element and U isotope analysis of uraninite and ore concentrate: applications for nuclear forensic investigations, Appl. Geochem. 84 (Supplement C) (2017) 277–285.
[5] T.L. Spano, et al., A novel nuclear forensic tool involving deposit type normalized rare earth element signatures, Terra. Nova 29 (5) (2017) 294–305.
[6] J. Mercadier, et al., Origin of uranium deposits revealed by their rare earth element signature, Terra. Nova 23 (4) (2011) 264–269.
[7] P. Alexandre, et al., Chemical compositions of natural uraninite, Can. Mineral. 53 (4) (2015) 595–622.
[8] K. Mayer, M. Wallenius, Z. Varga, Nuclear forensic science: correlating measurable material parameters to the history of nuclear material, Chem. Rev. 113 (2) (2013) 884–900.
[9] K. Mayer, M. Wallenius, I. Ray, Nuclear forensics—a methodology providing clues on the origin of illicitly trafficked nuclear materials, Analyst 130 (4) (2005) 433–441.
[10] E. Keegan, et al., The provenance of Australian uranium ore concentrates by elemental and isotopic analysis, Appl. Geochem. 23 (4) (2008) 765–777.
[11] Z. Varga, et al., Application of lead and strontium isotope ratio measurements for the origin assessment of uranium ore concentrates, Anal. Chem. 81 (20) (2009) 8327–8334.
[12] Z. Varga, M. Wallenius, K. Mayer, Origin assessment of uranium ore concentrates based on their rare-earth elemental impurity pattern, Radiochim. Acta Int. J. Chem. Aspect. Nucl. Sci. Technol. 98 (12) (2010) 771–778.
[13] V. Badaut, M. Wallenius, K. Mayer, Anion analysis in uranium ore concentrates by ion chromatography, J. Radioanal. Nucl. Chem. 280 (1) (2009) 57–61.
[14] A.L. de Souza, M.E.B. Cotrim, M.A.F. Pires, An overview of spectrometric techniques and sample preparation for the determination of impurities in uranium nuclear fuel grade, Microchem. J. 106 (Supplement C) (2013) 194–201.
[15] M. Cuney, The extreme diversity of uranium deposits, Miner. Deposita 44 (1) (2008) 3.
[16] F.J. Dahlkamp, Uranium deposits in collapse breccia pipes in the Grand Canyon region, Colorado Plateau, USA, Mitt, Naturwiss. Ver. Steiermark 120 (1990) 89–98.
[17] H.E. Frimmel, S. Schedel, H. Brätz, Uraninite chemistry as forensic tool for provenance analysis, Appl. Geochem. 48 (0) (2014) 104–121.
[18] R. Finch, T. Murakami, Systematics and paragenesis of uranium minerals, Rev. Mineral. 38 (1999) 91–180.
[19] J. Hardy C, The chemistry of uranium milling, Radiochim. Acta (1978) 121.
[20] Uranium Mining Overview, 2019. Available from: http://www.world-nuclear.org/information-library/nuclear-fuel-cycle/mining-of-uranium/uranium-mining-overview.aspx.
[21] I. Hore-Lacy (Ed.), Uranium for Nuclear Power: Resources, Mining and Transformation to Fuel. Woodhead Publishing Series in Energy, vol. 93, Elsevier, 2016.
[22] M.A. Floyd, R.W. Morrow, R.B. Farrar, Inductively coupled plasma-atomic emission spectroscopy: the determination of trace impurities in uranium hexafluoride, Spectrochim. Acta B Atom Spectrosc. 38 (1) (1983) 303–308.
[23] B.W. Short, H.S. Spring, R.L. Grant, Determination of Trace Impurities in Uranium Hexafluoride by an Inductively Coupled Argon Plasma Spectrometer, 1983 (United States).
[24] S.G. Brandberg, The conversion of uranium hexafluoride to uranium dioxide, Nucl. Technol. 18 (2) (1973) 177–184.
[25] K.C. Radford, J.M. Pope, UO2 fuel pellet microstructure modification through impurity additions, J. Nucl. Mater. 116 (2) (1983) 305–313.
[26] G.I. Park, et al., Effect of impurities on the microstructure of DUPIC fuel pellets using the SIMFUEL technique, Nuclear Engineering and Technology 40 (3) (2008) 191–198.
[27] C. Riglet-Martial, et al., Thermodynamics of chromium in UO2 fuel: a solubility model, J. Nucl. Mater. 447 (1) (2014) 63–72.
[28] W.B. Ferraz, et al., Effect of the W and MoO3 Additions on the Microstructure of UO2 Pellets, 2011.
[29] D. Ohai, Technologies for Manufacturing UO2 Sintered Pellets to Fuel Burnup Extension. Technical and Economic Limits to Fuel Burnup Extension, 2002, p. 193.
[30] N.A. Chorokov, Identification of unknown nuclear fuel by impurities and physical parameters, J. Radioanal. Nucl. Chem. 250 (1) (2001) 79–84.
[31] G.A. Brennecka, et al., Natural variations in uranium isotope ratios of uranium ore concentrates: understanding the 238U/235U fractionation mechanism, Earth Planet. Sci. Lett. 291 (1) (2010) 228–233.
[32] P. Alexandre, et al., Chemical compositions of natural uraninite, Can. Mineral. 53 (4) (2015) 595–622.
[33] P. Graves, Raman microprobe spectroscopy of uranium dioxide single crystals and ion implanted polycrystals, Appl. Spectrosc. 44 (10) (1990) 1665–1667.
[34] M. Fayek, et al., Micro-structures associated with uraninite alteration, J. Nucl. Mater. 277 (2–3) (2000) 204–210.
[35] J. Lv, et al., Raman scattering from phonons and electronic excitations in UO2 with different oxygen isotopes, J. Raman Spectrosc. 47 (3) (2016) 345–349.
[36] H. He, D. Shoesmith, Raman spectroscopic studies of defect structures and phase transition in hyper-stoichiometric UO 2+ x, Phys. Chem. Chem. Phys. 12 (28) (2010) 8109–8118.
[37] I.J. Schwerdt, et al., Uranium oxide synthetic pathway discernment through thermal decomposition and morphological analysis, Radiochim. Acta 107 (3) (2018).
[38] I.J. Schwerdt, et al., Nuclear forensics investigation of morphological signatures in the thermal decomposition of uranyl peroxide, Talanta 176 (2018) 284–292.
[39] A.M. Olsen, et al., Quantifying morphological features of α-U3O8 with image analysis for nuclear forensics, Anal. Chem. 89 (5) (2017) 3177–3183.
[40] P. Lucuta, et al., Thermal conductivity of SIMFUEL, J. Nucl. Mater. 188 (1992) 198–204.
[41] B. Santos, J. Noël, D. Shoesmith, The effect of pH on the anodic dissolution of SIMFUEL (UO2), J. Electroanal. Chem. 586 (1) (2006) 1–11.
[42] R. Verrall, P. Lucuta, Specific heat measurements of UO2 and SIMFUEL, J. Nucl. Mater. 228 (2) (1996) 251–253.
[43] B.W. Chung, R.G. Erler, N.E. Teslich, Three-dimensional microstructural characterization of bulk plutonium and uranium metals using focused ion beam technique, J. Nucl. Mater. 473 (2016) 264–271.
[44] W. Weber, Ingrowth of lattice defects in alpha irradiated UO2 single crystals, J. Nucl. Mater. 98 (1–2) (1981) 206–215.
[45] S. Imoto, Chemical state of fission products in irradiated UO2, J. Nucl. Mater. 140 (1) (1986) 19–27.
[46] B. Jeffery, Microanalysis of inclusions in irradiated UO2, J. Nucl. Mater. 22 (1) (1967) 33–40.
[47] G. Guimbretière, et al., Determination of in-depth damaged profile by Raman line scan in a pre-cut He2+ irradiated UO2, Appl. Phys. Lett. 100 (25) (2012) 251914.
[48] C.L. Tracy, et al., Review of recent experimental results on the behavior of actinide-bearing oxides and related materials in extreme environments, Prog. Nucl. Energy 104 (2018) 342–358.
[49] G. Nicolaou, Identification of unknown irradiated nuclear fuel through its fission product content, J. Radioanal. Nucl. Chem. 279 (2) (2009) 503–508.
[50] G.A. Jenner, et al., ICP-MS — a powerful tool for high-precision trace-element analysis in Earth sciences: evidence from analysis of selected U.S.G.S. reference samples, Chem. Geol. 83 (1–2) (1990) 133–148.
[51] A.D. Pollington, et al., Polyatomic interferences on high precision uranium isotope ratio measurements by MC-ICP-MS: applications to environmental sampling for nuclear safeguards, J. Radioanal. Nucl. Chem. 307 (3) (2016) 2109–2115.
[52] G. Manhes, J. Minster, C. Allegre, Comparative uranium-thorium-lead and rubidium-strontium study of the Saint Severin amphoterite: consequences for early solar system chronology, Earth Planet. Sci. Lett. 39 (1) (1978) 14–24.

[53] C.J. Bopp, et al., Uranium 238U/235U isotope ratios as indicators of reduction: results from an in situ biostimulation experiment at Rifle, Colorado, U.S.A, Environ. Sci. Technol. 44 (15) (2010) 5927.
[54] S. Richter, et al., Re-certification of a series of uranium isotope reference materials: IRMM-183, IRMM-184, IRMM-185, IRMM-186 and IRMM-187, Int. J. Mass Spectrom. 247 (1) (2005) 37–39.
[55] D.J. Condon, et al., Isotopic composition (238 U/235 U) of some commonly used uranium reference materials, Geochem. Cosmochim. Acta 74 (24) (2010) 7127–7143.
[56] S. Kappel, S.F. Boulyga, T. Prohaska, Direct uranium isotope ratio analysis of single micrometer-sized glass particles, J. Environ. Radioact. 113 (2012) 8–15.
[57] A. Simonetti, C. Gariépy, J. Carignan, Pb and Sr isotopic compositions of snowpack from Québec, Canada: Inferences on the sources and deposition budgets of atmospheric heavy metals, Geochem. Cosmochim. Acta 64 (1) (2000) 5–20.
[58] J. Janeczek, et al., Uraninite and UO2 in spent nuclear fuel: a comparison, J. Nucl. Mater. 238 (1) (1996) 121–130.
[59] C. Frondel, Systematic Mineralogy of Uranium and Thorium, vol. 1064, US Government Printing Office, 1958.
[60] M. Amme, et al., Raman microspectrometric identification of corrosion products formed on UO2 nuclear fuel during leaching experiments, J. Nucl. Mater. 306 (2–3) (2002) 202–212.
[61] D. Manara, B. Renker, Raman spectra of stoichiometric and hyper-stoichiometric uranium dioxide, J. Nucl. Mater. 321 (2–3) (2003) 233–237.
[62] ASTM, Standard Specification for Uranium Hexafluoride for Enrichment, 2018.
[63] D. Sangster, P. Outridge, W. Davis, Stable lead isotope characteristics of lead ore deposits of environmental significance, Environ. Rev. 8 (2) (2000) 115–147.
[64] J. Janeczek, R.C. Ewing, L.E. Thomas, Oxidation of uraninite: Does tetragonal U3O7 occur in nature? J. Nucl. Mater. 207 (1993) 177–191.
[65] B.D. Cullity, Elements of X-Ray Diffraction, Addison-Wesley Pub. Co, Reading, Mass, 1956.
[66] G.C. Allen, N.R. Holmes, Characterization of binary uranium oxides by infrared spectroscopy, Appl. Spectrosc. 48 (4) (1994) 525–530.
[67] G. Allen, J. Crofts, A. Griffiths, Infrared spectroscopy of the uranium/oxygen system, J. Nucl. Mater. 62 (2–3) (1976) 273–281.
[68] J.I. Bullock, Raman and infrared spectroscopic studies of the uranyl ion: the symmetric stretching frequency, force constants, and bond lengths, J. Chem. Soc., A, No. 5 (1969) 781–784.
[69] J.-G. Kim, et al., Infrared Spectra of Uranium Oxides Measured by ATR-FTIR, J. Nucl. Sci. Technol. 46 (12) (2009) 1188–1192.
[70] K. Satyanarayana, S. Durani, Separation and inductively coupled plasma optical emission spectrometric (ICP-OES) determination of trace impurities in nuclear grade uranium oxide, J. Radioanal. Nucl. Chem. 285 (3) (2010) 659–665.
[71] R.K. Malhotra, K. Satyanarayana, Estimation of trace impurities in reactor-grade uranium using ICP-AES, Talanta 50 (3) (1999) 601–608.
[72] M. Depiné, et al., Trace element distribution in uraninite from Mesoarchaean Witwatersrand conglomerates (South Africa) supports placer model and magmatogenic source, Miner. Deposita 48 (4) (2013) 423–435.
[73] H.C.S. GmbH, Product Information for Molybdenum and Tungsten for Nuclear Fuel Processing, 2019. Available from: https://www.hcstarck.com/nuclear_fuel_processing_products_mola_w.
[74] B.M. Ma, Nuclear Reactor Materials and Applications, Iowa State Univ, 1983.
[75] L.F. Van Swam, F. Garzarolli, H. Ruhmann, Zirconium Tin Iron Alloys for Nuclear Fuel Rods and Structural Parts for High Burnup, Google Patents, 1998.
[76] C. Degueldre, et al., Nuclear fuel in generation II and III reactors: research issues related to high burn-up, Energy Environ. Sci. 4 (5) (2011) 1651–1661.
[77] J. Arborelius, et al., Advanced Doped UO2 Pellets in LWR Applications, J. Nucl. Sci. Technol. 43 (9) (2006) 967–976.
[78] E.P. Agency, Locating and Estimating Air Emmisions from Sources of Chromium, U.S. Environmental Protection Agency, Research Triangle Park, North Carolina, USA, 1984.
[79] Commission, U.S.N.R. NRC Nuclear Reactor Concepts, 2018, 6/4/2018]; Available from: https://www.nrc.gov/reading-rm/training.html.
[80] W.L. Chenoweth, The uranium-vanadium deposits of the Uravan Mineral Belt and adjacent areas, Colorado and Utah, in: New Mexico Geological Society 32nd Annual Fall Field Conference Guidebook, 1981, pp. 165–170.
[81] P. Hostetler, R. Garrels, Transportation and precipitation of uranium and vanadium at low temperatures, with special reference to sandstone-type uranium deposits, Econ. Geol. 57 (2) (1962) 137–167.
[82] V. McLemore, W. Chenoweth, *Geology and uranium-vanadium deposits in the Salt Wash Member.* Morrison Formation, King Tutt Mesa area, San Juan County, New Mexico, in: New Mexico Geological Society Guidebook vol. 48, 1997, pp. 273–278.
[83] A.D. Weeks, Mineralogy and geochemistry of vanadium in the Colorado Plateau, J. Less Common Met. 3 (6) (1961) 443–450. United States Nuclear Regulatory Commission.